Porous texture evolution in Nomex-derived activated carbon fibers

(Journal of Colloid and Interface Science 253, 169-176, 2002)

S. Villar-Rodil[a, b], R. Denoyel[a], J. Rouquerol[a], A. Martínez-Alonso[b] and J.M.D. Tascón[b]

[a]*MADIREL (CNRS-Université de Provence), Site CTM, 26 rue du 141ème RIA, 13331 Marseille, Cedex 3, France.*

[b]*Instituto Nacional del Carbón, CSIC, Apartado 73, 33080 Oviedo, Spain.*

Abstract

In the present work, the textural evolution of a series of activated carbon fibers with increasing burn-off degree, prepared by the pyrolysis and steam activation of Nomex aramid fibers, is followed by measurements of physical adsorption of N_2 (77 K) and CO_2 (273 K) and immersion calorimetry into different liquids (dichloromethane, benzene, cyclohexane). The immersion calorimetry results are discussed in depth, paying special attention to the choice of the reference material. The activated carbon fibers studied possess an essentially homogeneous microporous texture, which suggests that these materials may be applied in gas separation, either directly or with additional CVD treatment.

Keywords: Activated carbon; Adsorption, Microcalorimetry; Immersion enthalpy, Microporosity.

1. Introduction

Due to their excellent adsorption properties, activated carbons play an outstanding role in many areas of modern science and technology, such as separation, purification and

catalysis (1, 2). In recent years, novel fibrous adsorbents known as activated carbon fibers (ACFs) have been developed by the pyrolysis and activation of organic fibers. ACFs have a number of advantages over the conventional activated granular/powdered carbons: high adsorption rates and capacity, a more homogeneous porous system which gives them greater adsorption selectivity, the possibility of their being molded into different shapes, etc.

In recent years, attempts have been made to obtain ACFs with novel porous texture characteristics. Thus, Freeman el al (3, 4) first reported on the outstanding homogeneity in pore size of ACFs prepared from highly ordered polymers, such as aramid fibers. Indeed, ACFs prepared from aramid show a narrower pore size distribution than those reported in the literature (5) for ACFs derived from more disordered precursors.

The high price of some aramid fibers prevents them from being used as feedstocks for obtaining carbonaceous adsorbents. However, previous works from one of the authors' laboratories (6, 7) have shown that low value by-products from the manufacture of aramid fibers can be an alternative option for the production of low cost ACFs. In addition, activated carbon yields are relatively high for these materials (8-10), so the process could be economically viable if the final adsorbents do offer advantages over the traditional ones. The textural properties of ACFs obtained through physical activation with carbon dioxide and steam using several varieties of aramid fibers as feedstocks have already been reported in the literature (4-7,11-13). However, little attention has been paid to the analysis of their pore size distribution. Moreover, to the authors' knowledge, no low relative pressure N_2 adsorption data on this type of materials has yet been reported. Obviously, a proper characterization of the porosity of these adsorbents is essential for their successful synthesis and application.

In this work, pyrolysis and physical activation with steam were carried out, using Nomex as starting material. Nomex (poly (*m*-phenylene isophthalamide)) is a particularly attractive precursor for obtaining very selective adsorbents, as it has been proved to yield fibrous adsorbents, whose porosity covers a narrow range in relation to other aramid fibers, making them promising molecular sieves (4, 7, 14). As for the use of steam as activating agent, it has been suggested that its utilization instead of carbon dioxide in the activation process of aramid fibers does not lead to a significant widening of the pore sizes (4), unlike the case of other carbonaceous materials (15, 16). In these conditions, steam is preferable to carbon dioxide from a practical point of view, due to its lower price and its higher reactivity towards carbon (lower temperatures can therefore be used for convenient activation rates, with the subsequent saving of energy).

The textural characterization of the samples has been focused in this work on the determination of their pore size distribution. With this aim, low relative pressure N_2 (77 K) as well as CO_2 (273 K) adsorption isotherms were measured in an attempt to elucidate pore size distributions indirectly by means of different calculation methods. Moreover, immersion calorimetry using adsorptive molecules of different size as molecular probes was employed to obtain a direct measurement of the amount of pores of different sizes. This technique has proved to be a useful tool for the characterization of microporous solids (16,17).

It is expected that these studies will help to predict in which separation processes these materials may be useful and whether it will be necessary to modify their textural characteristics with further treatments such as carbon chemical vapor deposition or other techniques to obtain valuable molecular sieve carbons.

2. Materials

The starting material was commercially available Nomex aramid fiber in a variety known as Crystalline Nomex (T450 2.2 dtex.). All treatments were carried out in a tubular quartz reactor. Batches of about 10 g of Nomex as received were pyrolyzed in argon (99.99990% pure by volume, flow rate: 50 cm^3 min^{-1}) up to 1073 K (heating rate: 10 K min^{-1}) and then cooled down to 1053 K and activated with a steam/argon mixture (720 cm^3 min^{-1} / 50 cm^{-3} min^{-1}) for various periods of time to attain different burn-offs (BO), namely, 0, 10, 21, 42 and 63%.

3. Methods

Adsorption isotherms of N_2 (77 K) and CO_2 (273 K) were assessed in a Micromeritics ASAP 2010 and a Quantachrome NOVA 1200 volumetric adsorption analyzer, respectively. With the help of a ASAP 2010 apparatus, it is possible to measure N_2 adsorption isotherms starting from relative pressures around 10^{-6}-10^{-7}, in order to obtain so-called "high resolution" N_2 adsorption isotherms. Samples were outgassed overnight under vacuum at 523 K prior to every adsorption experiment.

The heats of immersion of the samples into liquids with different minimal molecular dimensions such as dichloromethane (0.33 nm), benzene (0.37 nm) and cyclohexane (0.48 nm) were determined at 298 K with a Tian–Calvet differential microcalorimeter (Setaram, Model C80D). The samples (~0.1 g) were outgassed overnight under vacuum at 523 K. The experimental procedure to determine enthalpies of immersion has been described elsewhere (18).

The densities employed for adsorbed N_2 (77 K) and CO_2 (273 K) were 0.813 (bulk liquid) and 1.182 g cm^{-3} (solid phase) (19), respectively. BET surface areas, S_{BET}, were

obtained by the standard BET method in the relative pressure range from 10^{-6} to 0.1 (20). Total porosity ($V_{p\ (N2)}$) was calculated from the gas volume adsorbed at P/P^0=0.95.

Further insight into the textural evolution of the samples was gained through high resolution α_S-analysis, based on the original α_S method proposed by Gregg and Sing (21a) and reviewed for the high resolution adsorption isotherms by Kaneko (22). In this procedure, the adsorption isotherm for a given porous solid is expressed as a function of the amount adsorbed on a macroporous or non porous reference adsorbent. To do this, a parameter (α_S) is defined as the ratio of the amount adsorbed on the reference solid at each equilibrium relative pressure to the amount adsorbed at the relative pressure (0.4 for nitrogen) at which all the micropores are supposed to be already filled and the adsorbed amount is plotted as a function of α_S. External surface areas ($S_{ext\ (\alpha s,\ N2)}$) are calculated from the slope of the linear segment of the α_s plot corresponding to α_S higher than 1. Total micropore volumes ($V_{\mu p\ (\alpha s,\ N2)}$) as well as ultramicropore volumes ($V_{u\mu p\ (\alpha s,\ N2)}$) are obtained from the y-axis intercepts of the linear portions of the α_S plots corresponding respectively to the highest α_S values and to α_S of around 0.5. Spheron 6 carbon black (S_{BET}= 108 m^2g^{-1}), which has been shown to be equivalent to other reference materials offered in the literature as suitable for active carbons (23), was used as non porous standard.

Pore size distributions (PSDs) from the nitrogen adsorption data were obtained through the application of non local density functional theory (NLDFT) procedure (24) using a software provided by the Micromeritics Instrument Corporation. The NLDFT method for deriving PSDs is based on the assumption that experimental isotherms can be expressed as the sum of contributions from ideal isotherms calculated for adsorbate molecules on pores of fixed shape and size, the weighing function being equivalent to the PSD. Fluid-fluid interactions are accounted for using one-center Lennard-Jones potentials. The pores are modeled as an array of semi-infinite, rigid slits and their walls as

energetically uniform graphite. An analogous NLDFT method implemented for carbon dioxide (25), provided by Quantachrome, was used to obtain PSDs from the CO_2 adsorption data.

The accessible surface areas of the samples based on immersion calorimetry data were determined with the method proposed by Denoyel et al. (26), using as a reference the areal enthalpies of immersion of Vulcan 3 (S_{BET}= 82 m^2g^{-1}).

4. Results and Discussion

4.1. Nitrogen adsorption isotherms, comparative plots and derived PSDs. Fig. 1 shows the high resolution N_2 adsorption isotherms obtained for the samples under study. The adsorption isotherm of the pyrolyzed sample was not included in this figure because this material has a very narrow porosity, which is not accessible to N_2 at 77 K. As for the remaining samples, all their isotherms belong to type I according to the IUPAC classification (27), although distinctions can be established between them based on the widening of their knee as the burn-off increases. Whereas the isotherms of the low burn-off samples exhibit quite a sharp knee, reflecting the predominance of narrow microporosity (ultramicropores, i. e., pores with widths smaller than 0.7-0.8 nm), those corresponding to high burn-off degrees have a more rounded knee pointing to a widening of microporosity that even extends to mesoporosity in the sample activated to the highest burn-off, as shown by the appearance of a very narrow hysteresis loop in its isotherm.

To take full advantage of the information provided by the high resolution isotherm, the isotherms are represented on a semilogarithmic scale, as shown in Fig. 1b. Sing (21b) and Kaneko (22) pointed out that the pore filling process could be divided into three or

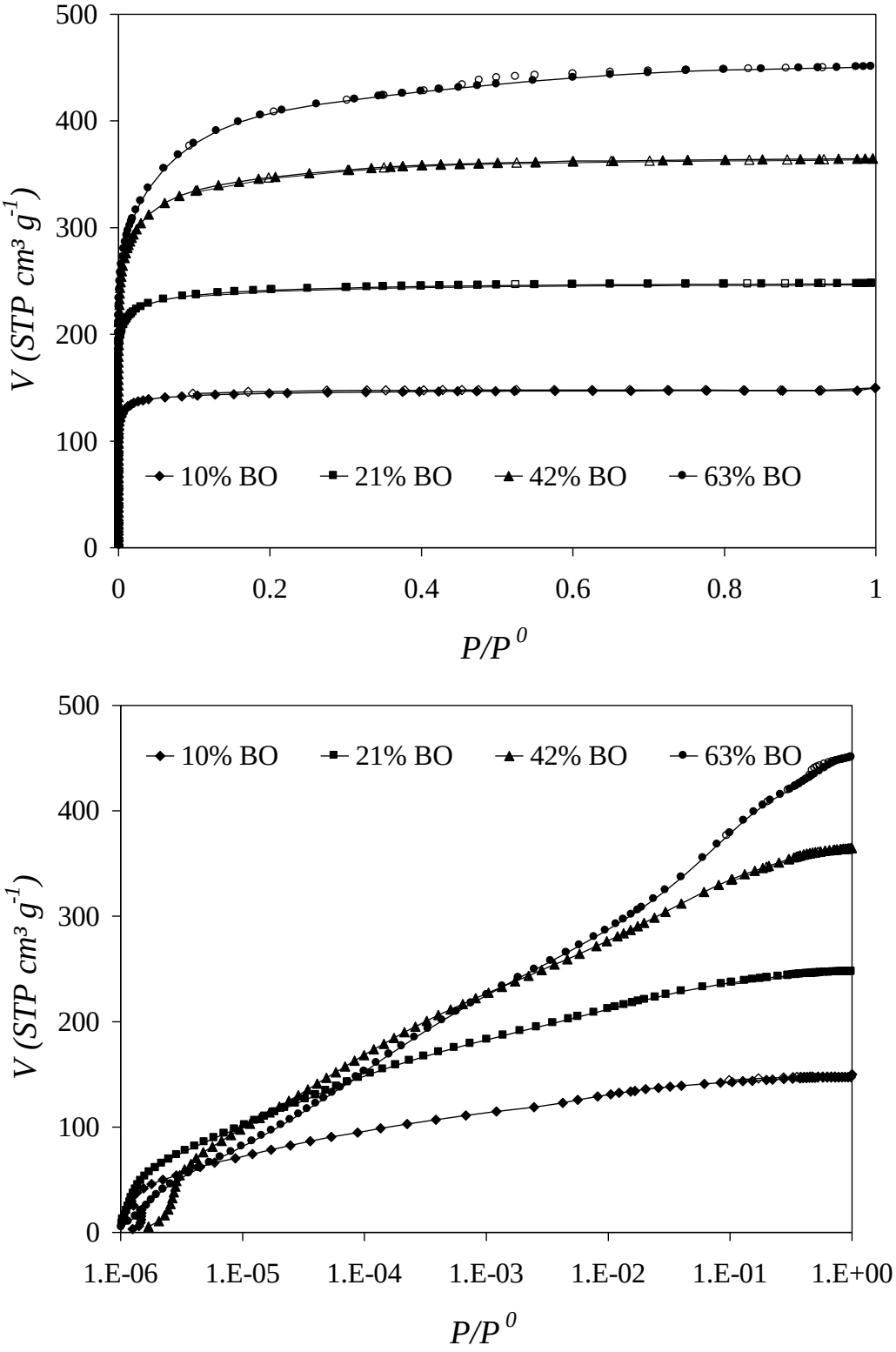

Figure 1. Adsorption-desorption isotherms of N_2 at 77 K. Filled symbols, adsorption; empty symbols, desorption. **(a)** Conventional plots; **(b)** Semilogarithmic scale

four stages: the filling of narrow micropores (ultramicropores), monolayer formation on the wider micropores (supermicropores) and small mesopores, the filling of mesopores by capillary condensation, and the filling of macropores by capillary condensation, which can be ascribed, respectively, to relative pressure ranges of ca. 10^{-6}-10^{-4}, 10^{-4}-10^{-2}, 10^{-2}-10^{-1}, and 0.9-1. Unlike conventional activated carbons (28) but like other ACFs (20, 29), all the samples in this work, even those activated to the highest BO, show a significant nitrogen uptake below $p/p^0=10^{-5}$, indicating the presence of a large amount of ultramicropores. However, the relative importance of the narrowest microporosity in the total porosity of the samples diminishes as BO increases. While ACFs activated to low BOs (10%, 21%) adsorb a large percentage of their total nitrogen uptake below $p/p^0=10^{-4}$, the uptake at the relative pressure range related to supermicropores (10^{-4}-10^{-2}) acquires significance for the ACFs activated to higher BOs (42%, 63 %), and even the appearance of a small amount of mesoporosity in the sample activated to 63% BO is reflected in the corresponding pressure range in its isotherm.

BET surface areas, S_{BET}, and total pore volumes, $V_{p\ (N2)}$, for the activated samples are given in Table 1. It can be seen that they increase systematically with the degree of burn-off over the range covered by this series. The very low relative pressures from which BET plots show linearity (~10^{-6}-10^{-5}) for all the samples are an indication of the highly microporous nature of their texture (30).

Table 1. Textural parameters derived from N_2 adsorption at 77 K.

% BO	S_{BET} ($m^2\ g^{-1}$)	$V_{p\ (N2)}$ ($cm^3\ g^{-1}$)	α_S method			
			$S_{ext\ (\alpha s,\ N2)}$ ($m^2\ g^{-1}$)	$V_{\mu p\ (\alpha s,\ N2)}$ ($cm^3\ g^{-1}$)	$V_{u\mu p\ (\alpha s,\ N2)}$ ($cm^3\ g^{-1}$)	$V_{u\mu p\ (\alpha s,\ N2)}/\ V_{\mu p\ (\alpha s,\ N2)}$
10	560	0.23	0.2	0.23	0.13	0.56
21	936	0.38	1.5	0.38	0.20	0.53
42	1329	0.56	2.7	0.56	0.18	0.32
63	1580	0.69	12.3	0.68	0.11	0.17

Regarding the α_S plot analysis, Kaneko *et al*. (22) found that microporous carbons could show two upward swings from linearity below the downward bending due to saturated filling at higher α_S, which they designated as filling swing (FS) and cooperative swing (CS), corresponding to α_S smaller and greater than 0.5, respectively. Both upward swings come from enhanced adsorbent-adsorbate interactions as a function of the pore size, and can be ascribed to different types of filling: primary micropore filling, which takes place in micropores whose width is less than two adsorbate molecular diameters, i.e., around 0.7-0.8 nm (ultramicropores (31)), for FS and cooperative adsorption in larger micropores (supermicropores) for CS.

The α_S plots derived from the N_2 adsorption data can be seen in Fig. 2. The two samples activated to the lowest BOs show mainly FS in the $0 < \alpha_S < 0.5$ range, with little evidence for CS, further confirming the view that ultramicropores are the dominant pores in these samples. On the other hand, the presence of both FS ($0 < \alpha_S < 0.5$) and CS ($0.5 < \alpha_S < 1$), in the two samples activated to the highest BOs is evidence of the existence of both ultramicropores and supermicropores. As burn-off increases, the FS, although still present, becomes less pronounced.

The textural parameters deduced from the application of the α_S method ($S_{ext\ (\alpha s,\ N2)}$, $V_{\mu p\ (\alpha s,\ N2)}$, $V_{u\mu p\ (\alpha s,\ N2)}$) are given in Table 1. A comparison of $V_{p\ (N2)}$ and $V_{\mu p\ (\alpha s,\ N2)}$ shows that both parameters follow the same rising trend with increasing burn off. These values coincide in all samples as might be expected given that most of their porosity is restricted to microporosity. The very small discrepancy for the sample with the highest BO (63%) indicates that mesoporosity is barely developed, as mentioned above. A quantitative estimate of the relative importance of the ultramicroporosity in the microporosity of the ACFs studied can be made from the ratio between $V_{u\mu p\ (\alpha s,\ N2))}$ and $V_{\mu p\ (\alpha s,\ N2)}$ given in Table 1. The progressive weakening of the FS with increasing burn-off is reflected in the

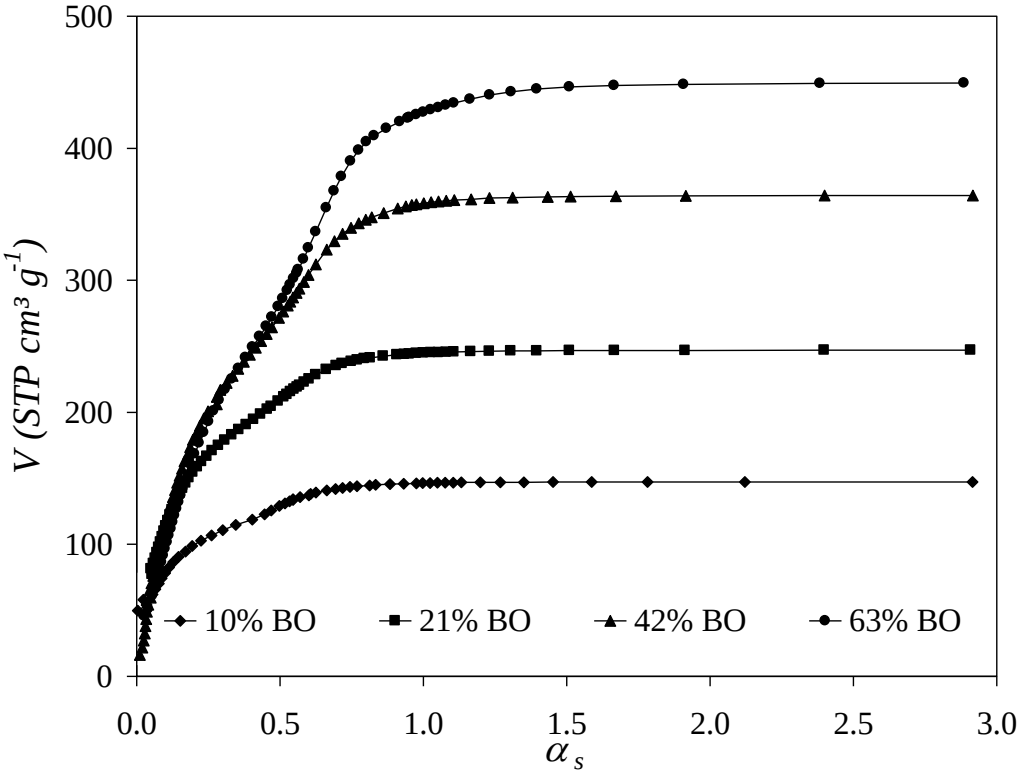

Figure 2. α_S plots drawn from N_2 adsorption isotherms for the series of activated carbon fibers.

decreasing value of this ratio. The low value found for the sample activated to the highest BO again indicates that porosity has significantly widened in this sample.

As regards the PSDs, NLDFT distributions for all samples (Fig. 3) present maxima at around 0.6 nm with pore sizes under 1.6, 2.0, 3.2 and 7.0 nm, respectively, for the samples arranged in an increasing burn-off sequence. The PSDs reflect a widening in the micropore size distribution. This takes place in a restricted pore size range below 2.0 nm, i.e. in the microporosity range, for all the samples except the one activated at 63% BO.

However, it is known that the NLDFT method is not totally reliable as a tool for yielding PSDs as it has model-induced artifacts (31). The rigid parallel wall model used to build the theoretical adsorption isotherms exhibits strong packing effects which are not

present in real activated carbons. As a consequence, the resulting pore size distributions consistently show two minima at around 0.6 and 1 nm, corresponding to the transitions from pore widths accommodating one adsorbed layer to two, and two layers to three, respectively. This feature is confirmed in Fig. 3.

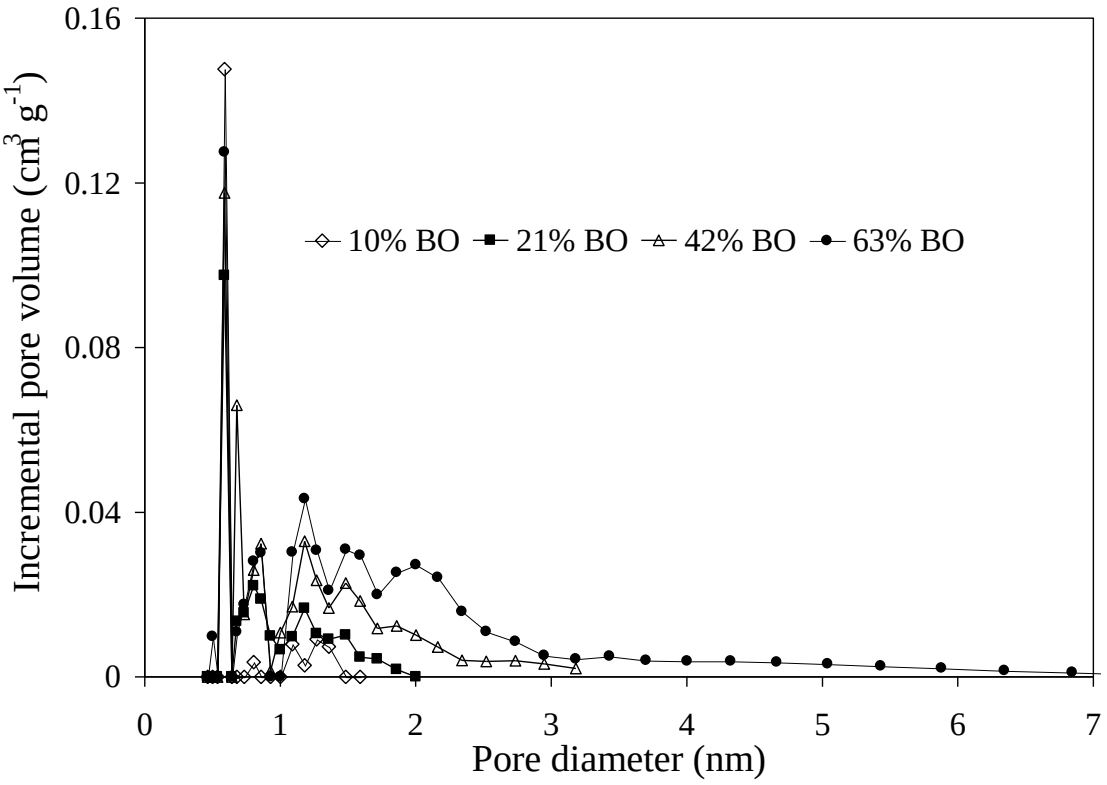

Figure 3. PSDs obtained from the N_2 adsorption isotherms through application of the NLDFT method.

4.2. Carbon dioxide isotherms, Dubinin-Radushkevich plots and derived PSDs. Carbon dioxide at 273 K and at subatmospheric pressures is known to cover only the microporosity range from around 0.3 nm to about 1.4 nm (25). On the other hand, a lower cut-off pore width of around 0.4 nm is generally assumed for nitrogen adsorption at 77 K owing to restricted diffusion. Thus, it has been suggested that the adsorption of these two

molecules should be used in a complementary way in order to characterize micro and mesoporosity more fully (33).

Fig. 4 shows the CO_2 adsorption isotherms for pyrolyzed and steam activated Nomex. Although the characterization by nitrogen adsorption at 77 K of the pyrolyzed sample was not possible, CO_2 adsorption at a higher temperature (273 K) serves as a useful tool for samples with narrow microporosity such as this one. At the early stages of activation, the CO_2 uptake increases over the entire relative pressure range covered, as can be confirmed by comparing the isotherms for the pyrolyzed and 10% BO activated samples. Although the total uptake at P/P^0=0.03 increases upon activation, a decrease in the uptake at low pressures is observed for further activated samples, reflecting the disappearance of some of the narrowest microporosity. Finally, the sample activated at the highest burn off even evidences a decrease in CO_2 total uptake, probably because high degrees of activation lead to the elimination of some of the pore walls in narrow micropores, thereby decreasing the amount of micropores enclosed in the range covered in these conditions.

The Dubinin-Radushkevich (DR) plots and textural parameters such as micropore volume ($V_{\mu p\ (DR,\ CO2)}$) and adsorption energy E_0, calculated through the application of the DR equation to CO_2 adsorption data, are shown in Fig. 5 and Table 2 respectively. Straight lines typical of microporous solids were obtained. The plot is linear over the whole range of relative pressures measured for the pyrolysed sample as well as for that activated to 10% BO. The fact that the former required longer times to reach equilibrium reflects a certain molecular restriction to the access of CO_2 to the pores in these conditions. The range of linearity decreases for the rest of the samples. In fact, the sample activated to 63% BO shows two linear branches from which two different values of $V_{\mu p\ (DR,\ CO2)}$ could have been calculated. This is further confirmation of the widening of micropore size distribution as the burn-off increases, resulting in different filling mechanisms for

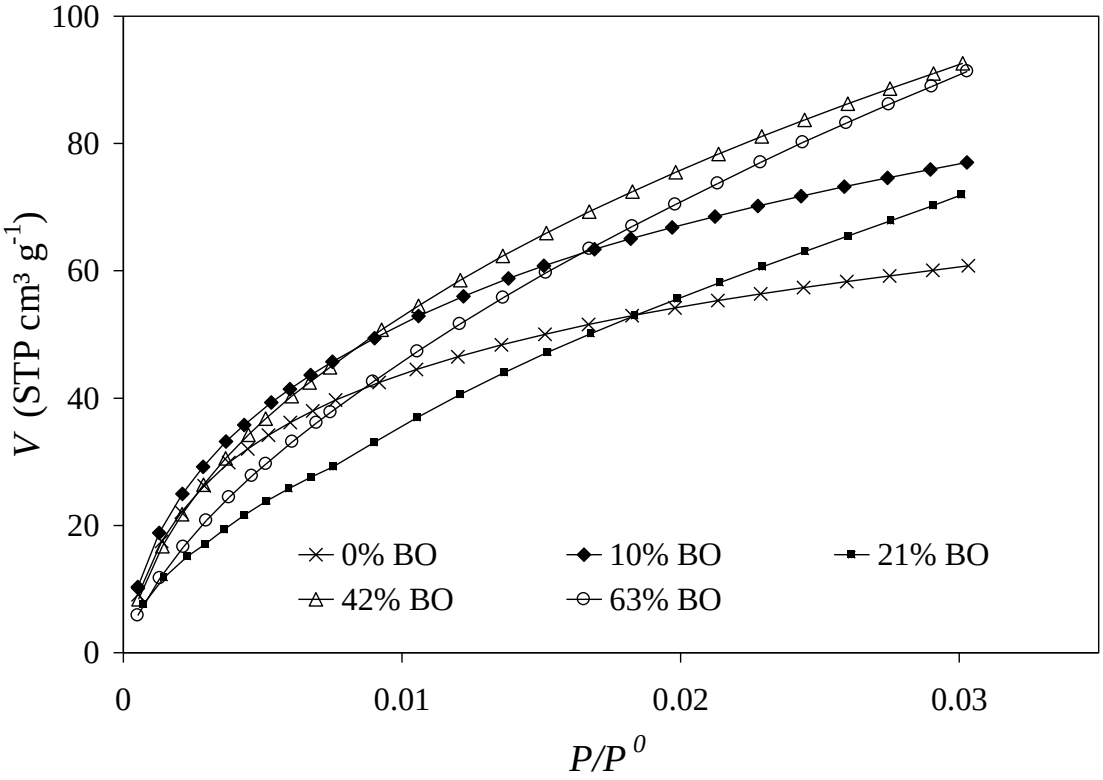

Figure 4. Adsorption isotherms of CO_2 at 273 K on carbonized Nomex and ACFs prepared from it by steam activation.

micropores of different size. Concerning the trends for the different parameters derived from the DR method, $V_{\mu p\ (DR,\ CO2)}$ increases as E_0 decreases, indicating that the microporosity range covered, (ultramicroporosity), develops through the widening of the pores. However, the nitrogen adsorption data suggested that the development of microporosity as a whole in Nomex-derived ACFs mainly involves the creation of new micropores and/or the deepening of pre-existing ones, widening being a relatively minor contribution in comparison with ACFs derived from other precursors. It must been taken into account that nitrogen adsorption covers a wider range of porosity than carbon dioxide, thus offering a more general picture of textural evolution.

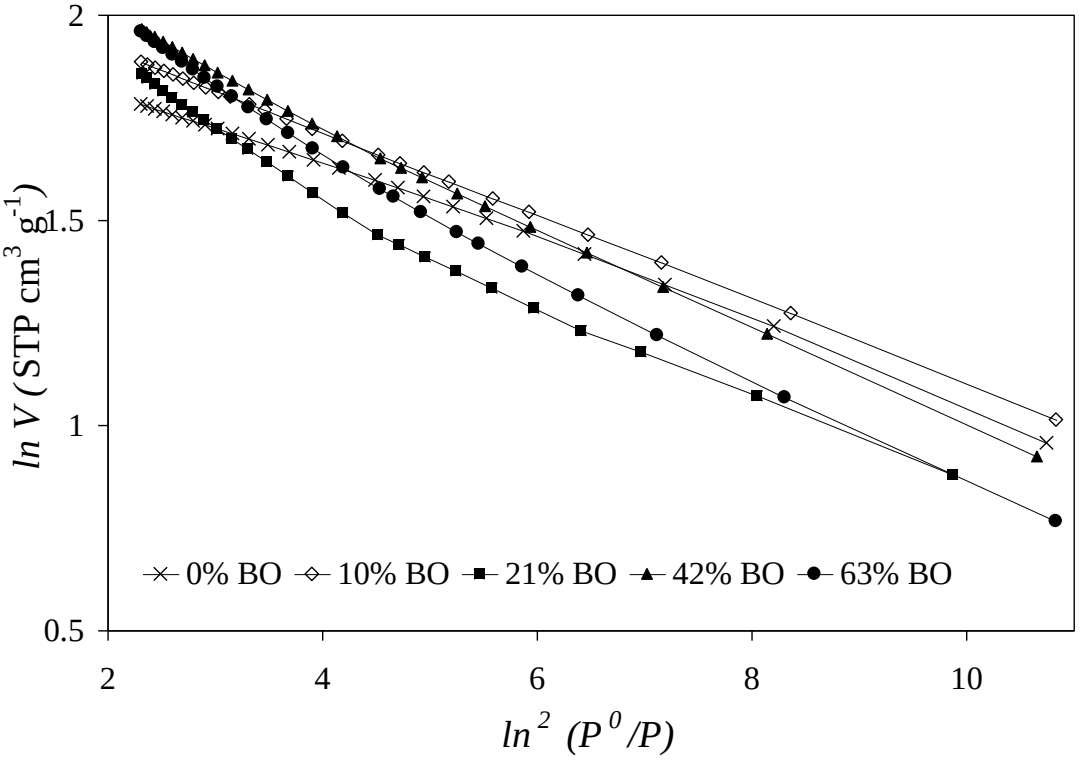

Figure 5. DR plots obtained from the CO_2 adsorption data.

Table 2 Textural parameters calculated through the application of the DR equation to CO_2 adsorption data at 273 K.

% BO	DR method	
	$V_{\mu p\ (DR,\ CO2)}$ ($cm^3\ g^{-1}$)	E_0 ($KJ\ mol^{-1}$)
0	0.16	27.5
10	0.22	25.7
21	0.26	20.7
42	0.29	23.1
63	0.38	19.5

The comparison of $V_{\mu p\ (\alpha s,\ N2)}$ determined by N_2 adsorption (through the α_S method) with $V_{\mu p\ (\mathrm{DR},\ CO2)}$ determined by CO_2 adsorption (through the DR method) can provide useful information about the texture of the samples (32). The already discussed results from applying the α_S method to N_2 adsorption were found to be equivalent to those derived from the application of the DR method to the same data (not shown to avoid duplication), which is why they are used here. When comparing $V_{\mu p\ (\alpha s,\ N2)}$ with $V_{\mu p\ (\mathrm{DR},\ CO2)}$, three different situations typically arise as pores widen. The first situation, in which $V_{\mu p\ (\alpha s,\ N2)} < V_{\mu p\ (\mathrm{DR},\ CO2)}$, appears for the pyrolyzed sample. This situation usually occurs in molecular sieve carbons, carbonized materials or activated carbons with a very low burn-off (30). If, as already mentioned, carbon dioxide adsorption in these conditions starts from the smallest pore widths, around 0.3 nm, while nitrogen adsorption is restricted to pores wider than 0.4 nm, the volume of micropores with widths between 0.3 and 0.4 nm can be roughly estimated by subtracting $V_{\mu p\ (\alpha s,\ N2)}$ from $V_{\mu p\ (\mathrm{DR},\ CO2)}$. In the case of the pyrolyzed sample studied in this work, no nitrogen at all was adsorbed, i. e., $V_{\mu p\ (\alpha s,\ N2)}=0$, reflecting the fact that all the pores belong to the pore width interval, which is optimum for the separation of gas mixtures such as CO_2(0.33 nm)/CH_4(0.38 nm) and O_2(0.346 nm)/N_2(0.364 nm) (14). Consequently, the pyrolyzed sample could in principle serve as a good molecular sieve, al least from the point of view of selectivity. The usual argument against the use of simply pyrolyzed carbonaceous materials as molecular sieves is their low adsorption capacity. However, this is not the case here, as the micropore volume of the sample ($V_{\mu p\ (DR,\ CO2)}$=0.16 $cm^3\ g^{-1}$) is well inside the range of those exhibited by commercial and non-commercial carbon molecular sieves in the literature (34, 35). Moreover, the densities used in the literature for CO_2 adsorbed at 273 K are typically lower than the one used in this work and consequently the values calculated for micropore volumes are “inflated” in relation with ours.

The second situation, $V_{\mu p\ (\alpha s,\ N2)} \sim V_{\mu p\ (\mathrm{DR,\ CO2})}$, arises for the sample activated to 10% BO and is the usual situation for some molecular sieves and activated carbons with a low or intermediate burn-off. As micropore volumes derived from nitrogen and carbon dioxide adsorption isotherms are practically identical for the 10% BO sample, all the porosity is restricted to microporosity, as in the first situation, but in this case the pores must have widened. If there are any pores left in the 0.3-0.4 nm range, only filled by CO_2 adsorption, in order that both volumes become equal, some development of microporosity must have occurred beyond the pore widths of 1.4 nm, covered exclusively by N_2.

The third situation, when $V_{\mu p\ (\alpha s,\ N2)} > V_{\mu p\ (\mathrm{DR,\ CO2})}$ is found for the remaining samples and implies the continued development of porosity beyond the upper limit of 1.4 nm covered by CO_2 adsorption. This is typical of activated carbons with a relatively high burn-off.

As for the possible use of the activated samples studied in this work, their rather small and uniform pore sizes make them promising CMS precursors through carbon chemical vapor deposition (36). Nevertheless, the sample activated to the highest burn-off shows mainly wide micropores, as shown above by the low $V_{u\mu p\ (\alpha s,\ N2)}$ to $V_{\mu p\ (\alpha s,\ N2)}$ ratio, which even extends to mesopores (from the small hysteresis loop found in its isotherm). This makes its possible application even as a precursor of carbon molecular sieves doubtful. Moreover, such a high burn-off is hardly admissible from a practical point of view due to excessive carbon consumption.

Incremental pore volume plots calculated from CO_2 adsorption (NLDFT method) for all the samples are shown in Fig. 6. As the calculation procedure is analogous to that applied to nitrogen adsorption data, an artificial minimum at around 0.6-0.7 nm, related to the ideal transition from one to two layers of adsorbate, is also found systematically. The next transition from two to three layers is not appreciated in the relative pressure range

extending to atmospheric pressure (25). The PSDs are represented up to the limit of sensitivity of CO_2 adsorption, in these conditions fixed at 1 nm, as theoretical isotherms for solids with pores greater than 1 nm are linearly dependent and, consequently, these pores cannot be distinguished.

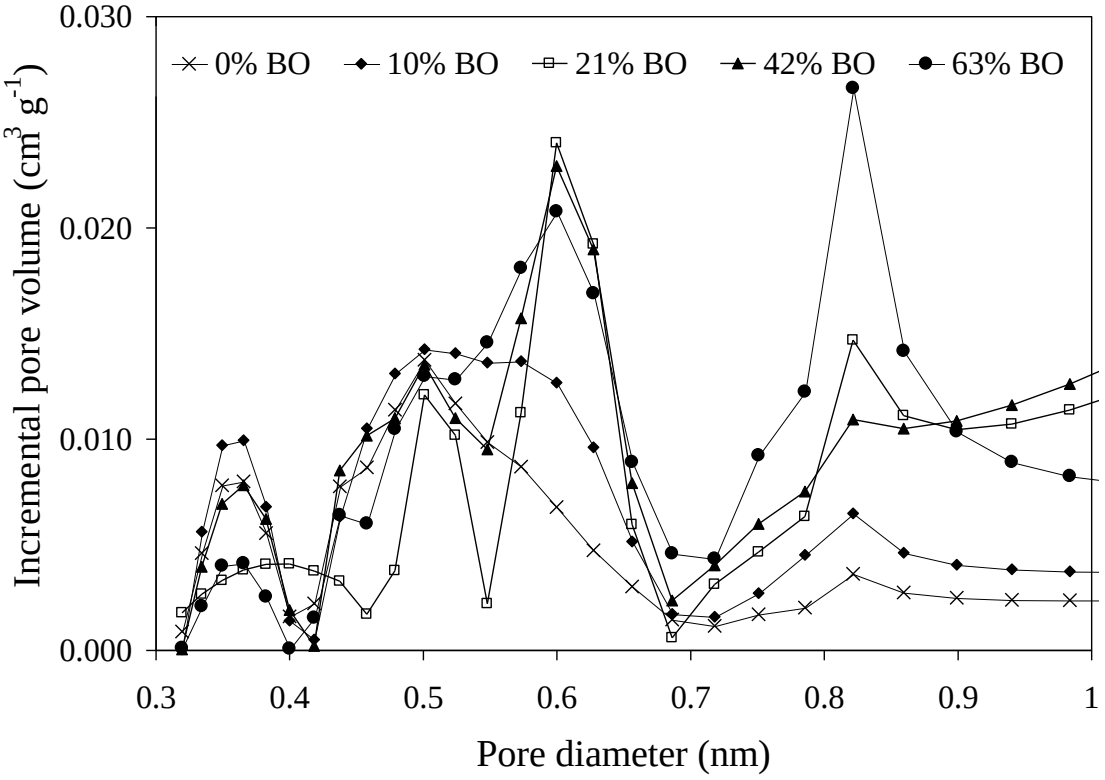

Figure 6. PSDs obtained from the CO_2 adsorption isotherms through application of the NLDFT method.

As can be seen in Fig. 6, the pyrolyzed sample shows maxima at 0.35 and 0.50 nm which are also present in the activated samples. But as burn-off increases, the former disappears while the latter is gradually hidden, already at 10% BO, by the appearance of another maximum at 0.6 nm. For the most activated samples, the maximum for the PSDs occurs at 0.82 nm. Consequently, in the porosity range covered by CO_2 adsorption, widening of the pores can also be appreciated, as samples would have maxima for their

PSDs at around 0.35 and 0.50 nm (0% BO), 0.50-0.60 nm (10% BO), 0.60 nm (21% and 42% BO) and 0.82 nm (63% BO).

4.3. Immersion calorimetry measurements. As calculation methods based on data from a single isotherm do not seem to be totally reliable, it was thought advisable to employ adsorptive molecules of different sizes as molecular probes to assess the different stages of micropore filling in a direct way (37) through immersion calorimetry experiments.

A comparison of the different proportionality factors between the heats of immersion and surface areas obtained for a number of reference materials is given in Table 3. As can be seen, the values of specific surface areas derived from immersion data may vary significantly depending on the choice of the reference material. For example, the surface area of a material derived from its heat of immersion into C_6H_6 using Spheron 6 would be almost twice the value obtained using Reference1. As Spheron 6 is an extreme case, with the highest ratio of heat of immersion to surface area, Vulcan 3 was finally chosen as the reference to calculate specific surface areas derived from the immersion calorimetry data measured in this work.

Table 4 shows the experimental enthalpies of immersion in the various organic liquids studied of all the samples except for the one activated to the highest burn-off together with the calculated accessible surface areas. This sample (63 % BO) was useful for setting an upper limit for developing of exclusively microporosity through activation, but it has been excluded from further analysis because it is not of interest for possible application as a molecular sieve carbon.

The samples activated to low BOs (0 and 10 % BO) show surface areas accessible to dichloromethane higher than those accessible to benzene. However, the rest of the

samples show the opposite trend. This change in the activation series could be explained in terms of an evolution of the surface chemistry of the pyrolyzed sample, as activation takes place by way of the loss of surface functional groups, the appetence for polar molecules such as dichloromethane decreasing. Nevertheless, generally speaking, chemical factors are not thought to be important in an adsorption process like this (11, 40, 41).

Table 3. Ratios between the enthalpy of immersion at 298 K into the three liquids used in this work and the BET surface area for different reference materials.

	Ratio (mJ m^{-2})			
	Reference1[a] (50 m^2 g^{-1})	Vulcan 3G[b] (62 m^2 g^{-1})	Vulcan 3[c] (82 m^2 g^{-1})	Spheron 6[c] (108 m^2 g^{-1})
CH_2Cl_2	63	113	134	170
C_6H_6	76	114	111	148
C_6H_{12}	60	104	104	101

[a] Calculated from data in ref. 38.

[b] Calculated from data in ref. 39.

[c] This work.

Table 4. Experimental enthalpies of immersion at 298 K into different liquids and surface areas derived from them and from N_2 adsorption at 77 K.

% BO	$-\Delta H_{imm}$ (J g^{-1})			Surface areas (m^2 g^{-1})			S_{BET} (m^2 g^{-1})
	CH_2Cl_2	C_6H_6	C_6H_{12}	CH_2Cl_2	C_6H_6	C_6H_{12}	
0	45.3	11.0	10.0	338	100	96	-[a]
10	92.1	65.9	47.6	687	600	460	560
21	123.1	122.4	81.6	918	1116	787	936
42	138.1	146.7	107.6	1029	1337	1038	1329

[a] Only geometrical surface

Surface areas accessible to benzene are systematically higher than the corresponding BET surface areas. As the minimal dimensions of nitrogen (0.36 nm) and benzene (0.37 nm) are nearly the same, both molecules should have access to similar microporosity ranges. It has been asserted (26) that differences such as this arise from the underestimation of the actual surface area of microporous carbons whose pores have widths similar to one adsorbate molecule by the calculation of BET surface area. This underestimation occurs because one molecule is only considered to be in contact with only one planar surface. In the immersion method, the interaction of the molecule with both walls of the pore is taken into account giving higher, more realistic values. Accordingly, the biggest differences between the surface areas derived from nitrogen and benzene adsorption would appear in the samples with the narrowest porosities that are accessible to both molecules. This trend can be verified in the series studied as the differences between the two surface areas decrease with increasing burn-off, differences barely being noticeable in the sample activated to 42% BO. It was previously shown in discussing parameters calculated by the α_S method that the contribution of ultramicropores to the microporosity of this sample is smaller than for the samples activated to lower BOs. At 42% BO, the microporosity has widened to the point that almost all the pores can accommodate more than one molecule of nitrogen, so that the hypothesis of the BET surface is acceptable in this case.

For the next probe molecule, cyclohexane, the values for accessible surface areas are lower than the BET surface areas for all the samples except the pyrolyzed one, indicating a molecular sieve effect. The different sizes of nitrogen (0.36 nm) and cyclohexane (0.48 nm) molecules justify the differences as the bigger molecules will have access to a smaller range of microporosity in the samples. However, for the pyrolyzed sample, the surface area accessible to cyclohexane is higher than the BET surface area

(assuming this to be the geometrical area). The porosity in this sample is probably so narrow that the leading factor is the underestimation of the area calculated from N_2 adsorption which, at 77 K, has restricted diffusion limitations in the pores of molecular dimensions. As a result, the difference in the size of the two molecules is counterbalanced.

5. Summary

It can be deduced from the different analyses performed that the microporosity developed in the samples studied through activation is mainly restricted to pores between one and two molecular diameters (of N_2 or C_6H_6), i. e. ultramicropores. Nevertheless, there is a qualitative change between the two samples activated to lower burn-offs (0 and 10 %) and the other samples. Ultramicropores are the dominant micropores in the former while supermicropores gain significance in the latter.

The absolute values for specific surface areas derived from immersion calorimetry measurements are highly dependent on the reference material chosen. This must be taken into account when comparing with other values in the literature or with BET (N_2) surface areas.

Acknowledgements

The authors wish to thank their colleagues Javier Fernández and Celina Blanco (DuPont Asturias) for providing the Nomex sample. Financial support from CICYT (Project 1FD1997-1915) is gratefully acknowledged. We also acknowledge a predoctoral fellowship from the Spanish Ministry of Education awarded to S.V.-R., which allowed her to carry out a stay at MADIREL (CNRS-Université de Provence).

References

(1) Bansal, C. R., Donnet, J. B. and Stoeckli F., "Active Carbon." Marcel Dekker, New York, 1988.

(2) Derbyshire, F., Jagtoyen, M., Andrews, R., Rao, A., Martín-Gullón, I. and Grulke, E.A., "Carbon materials in environmental applications" *in* "Chemistry and Physics of Carbon", (L. R. Radovic., Ed.), vol. 27, pp. 1-66. Marcel Dekker, New York, 2001.

(3) Freeman, J. J., Tomlinson, J. B., Sing, K. S. W. and Theocharis, C. R., *Carbon* **6**, 865 (1993).

(4) Freeman, J. J., Tomlinson, J. B., Sing, K. S. W. and Theocharis, C. R., *Carbon* **33**, 795 (1995).

(5) Matsumoto, A., Zhao J. and Tsutsumi K., *Langmuir* **13**, 496 (1997).

(6) Martínez-Alonso, A., Jamond, M., Montes-Morán, M. A. and Tascón, J. M. D., *Microporous Mater.* **11**, 303 (1997).

(7) Blanco López, M., Villar-Rodil, S. M., Martínez-Alonso, A. and Tascón, J. M. D., *Microporous Mesoporous Mater.* **41**, 319 (2000).

(8) Mosquera, M. E. G., Jamond, M., Martínez-Alonso, A. and Tascón, J. M. D., *Chem. Mater.* **6**, 1918 (1994).

(9) Villar-Rodil, S. M., Martínez-Alonso, A. and Tascón, J. M. D., *J. Anal. Appl. Pyrolysis* **58-59**, 105 (2001).

(10) Villar-Rodil, S. M., Paredes, J. I., Martínez-Alonso, A. and Tascón, J. M. D., *Chem. Mater.* **13**, 4297 (2001).

(11) Stoeckli, F., Centeno, T.A., Fuertes, A. B. and Muñiz, J., *Carbon* **34**, 1201 (1996).

(12) Blanco López, M.C., Martínez-Alonso, A. and Tascón, J. M. D., *Microporous Mesoporous Mater.* **34**, 171 (2000).

(13) Blanco López, M.C., Martínez-Alonso, A. and Tascón, J. M. D., *Carbon* **38**, 1173 (2000).

(14) Freeman, J. J., Gimblett, F. G., Hayes, R. A., Amin, Z. M. and Sing, K. S. W. *in* "Characterization of Porous Solids II" (F. Rodríguez-Reinoso et al., Eds.), p. 366. Elsevier, Amsterdam, 1991.

(15) Ryu, S. K., Jin, H., Gondy, D., Pusset, N. and Ehrburger, P., *Carbon* **31**, 841 (1993).

(16) Molina-Sabio, M., González, M. T., Rodríguez-Reinoso, F. and Sepúlveda-Escribano, A., *Carbon* **34**, 505 (1996).

(17) Silvestre-Albero, J., Gómez de Salazar, C., Sepúlveda-Escribano, A. and Rodríguez-Reinoso, F., *Colloids Surf. A* **187-188**, 151 (2001).

(18) Partyka, S., Rouquerol, F. and Rouquerol, J., *J. Colloid Interface Sci.* **68**, 21 (1979).

(19) Cascarini de Torre, L. E., Bottani, E. J. and Steele, W. A., *Langmuir* **12**, 5399 (1996).

(20) Ryu, Z., Zheng, J., Wang, M. and Zhang, B., *J. Colloid Interface Sci.* **230**, 312 (2000).

(21) Gregg, S. J. and Sing, K. S. W., "Adsorption, Surface area and Porosity." (a) p. 94, (b) p. 242. Academic Press, London, 1982.

(22) Kaneko, K., Ishii, C., Ruike, M. and Kuwabara, H., *Carbon* **30**, 1075 (1992).

(23) Setoyama, N., Suzuki, T. and Kaneko, K., *Carbon* **36**, 1459 (1998).

(24) Olivier, J. P., Conkin, W. P. B. and Szombathely, M. V. *in* "Characterization of Porous Solids III" (J. Rouquerol, F. Rodríguez-Reinoso, K. S. W. Sing and K. K. Unger, Eds.), p.81. Elsevier, Amsterdam, 1994.

(25) Vishnyakov, A., Ravikovitch, P. I. and Neimark, A. V., *Langmuir* **15**, 8736 (1999).

(26) Denoyel, R., Fernandez-Colinas, J., Grillet, Y. and Rouquerol, J., *Langmuir* **9**, 515 (1993).

(27) Sing, K. S. W., Everett, D. H., Haul, R. A. W., Moscou, L., Pieriotti, R. A., Rouquerol, J. and Siemieniewska, T., *Pure Appl. Chem.* **57**, 603 (1985).

(28) Dombrowski, R. J., Hyduke, D. R., Lastoskie, C. M., *Langmuir*, 16, 5041 (2000).

(29) Li, Z., Kruk, M., Jaroniec, M., Ryu, S. K., *J. Colloid Interface Sci.* **204**, 151 (1998).

(30) Rouquerol, F., Rouquerol, J. and Imelik, B., *Bull. Soc. Chim. Fr*. 635 (1964).

(31) Dubinin, M. M., *Prog. Surf. Membrane Sci.* **9**, 1 (1975).

(32) Olivier, J. P., *Carbon* **36**, 469 (1998).

(33) Garrido, J., Linares-Solano, A., Martín-Martínez, J. M., Molina-Sabio, M., Rodríguez-Reinoso, F. and Torregrosa, R., *Langmuir* **3**, 76 (1987).

(34) De la Casa-Lillo, M. A., Alcañiz-Monge, J., Raymundo-Piñero, E., Cazorla-Amorós, D. and Linares-Solano, A., *Carbon* **36**, 1353 (1998).

(35) Reid, C. R., O'Koye, I. P. and Thomas K. M., *Langmuir* **14**, 2415 (1998).

(36) Freitas, M. M. A. and Figueiredo, J. L., *Fuel* **80**, 1 (2001).

(37) Sing, K. S. W., *Adv. Colloid Interface Sci.* **76-77**, 3 (1998).

(38) Manso, R., "Preparación de tamices moleculares de carbono a partir de carbones minerales", Salamanca, Spain: University of Salamanca, 1999, Ph. D. Thesis.

(39) Gómez-de-Salazar, C., "Desarrollo de tamices moleculares de carbón para la separación de mezclas de gases", Alicante, Spain: University of Alicante, 2000, Ph. D. Thesis.